Seismological Research Letters

Performance of the GFZ Decentralized On-Site Earthquake Early Warning Software (GFZ-Sentry): Application to K-NET and KiK-Net Recordings, Japan

by Stefano Parolai, Adrien Oth, and Tobias Boxberger

ABSTRACT

In this article, we report on the application of GFZ-Sentry software for decentralized on-site earthquake early warnings to a large data set of recordings collected by the Japanese K-NET and KiK-net seismic networks. The data set is composed of 3,225 three-component recordings from 24 seismic events. The magnitudes of the selected earthquakes fall into a range of M_{JMA} 6.0–7.3 (M_w 5.7–6.9) and cover hypocentral (epicentral) distances between 5 and 107 km (2 and 103 km, respectively). The data have been coordinated in real time with velocity and displacement; in this manner, the peak ground displacement (Pd) within the first few seconds (to a maximum of 3 s) after the P-wave arrival in the vertical component is determined. This value is used to estimate the peak ground velocity (the median, along with the associated 16% and 84% confidence intervals) on the horizontal components using empirical relationships. Based on these values, the traffic light status (green, orange, red) is then determined following the methodology introduced by Parolai et al. (2015), which uses three matrices to show the relationship between the expected ground motion and the possible damage (in terms of seismic intensity) that may arise. The performance of the software was evaluated without making *ad hoc* calibrations for the area or the selected thresholds and was found to be quite reliable.

For example, in 90% of cases, assignment of the "red" status is followed by shaking that leads to a seismic intensity equal to or greater than V (very light potential damage). Additionally, all of the recordings leading to an intensity greater than VII (moderate to heavy damage) were correctly classified by a red status. Similarly, when considering all the declared green statuses, it is remarkable that only in 10% of cases was there a "missed alarm" (i.e., a green status is determined, but due to the level of observed shaking, it is later seen that the status should have been red).

INTRODUCTION

In recent years, significant advances have been made in the development of earthquake early warning (EEW) systems in various earthquake-prone regions around the world (e.g., Clinton et al., 2016; Oth and Parolai, 2016), because these systems have been recognized as potentially valuable tools for mitigating the risks associated with strong earthquakes (e.g., Wenzel and Zschau, 2014). Recent studies have also highlighted the cost effectiveness and social benefit of EEW systems (Strauss and Allen, 2016; Woo et al., 2016).

In addition, the improvement in low-cost sensors has allowed for the further development of innovative approaches for decentralized on-site early warning systems (with a single station as the base), as well as risk-based early warning systems (Bindi et al., 2015, 2016) that allow for rapid loss assessments. These assessments support the decision-making process as to whether or not to issue a warning before the ground motions reach a target site. Within the framework of real-time and near-real-time risk assessment, such systems may also be combined with immediate post-event response evaluations that are based on recorded shaking (monitoring) and short-term aftershock risk management for automated building tagging.

Parolai et al. (2015) proposed recommendations on what types of data processing software should be employed for efficiently carrying out decentralized on-site early warning (DOSEW) tasks (e.g., on carrying out event detection using a low-pass filtered version of the signal and on how to design the alarm based on matrices filled with the real-time ground-motion forecasts). These recommendations were accommodated during the design of the GFZ-Sentry software, which is currently running as a part of the real-time strong-motion networks that the Helmholtz Centre Potsdam GFZ German Research Centre for Geosciences (GFZ) operate in cooperation with local partners (see Data and Resources). In DOSEW, both the required computations and the decisions with regard to issuing alarms are made on-site.

In this article, we present the results of an extensive application of the GFZ-Sentry algorithm to a data set that is composed of recordings from the Japanese K-NET and the KiK-net networks. Collectively, these networks are the result of large-scale efforts devoted to the establishment of dense

and uniformly spaced strong-motion, highly sensitive, and broadband seismic networks throughout Japan (Fujiwara *et al.*, 2004; Okada *et al.*, 2004; Aoi *et al.*, 2011) following the devastating January 1995 Kobe earthquake (e.g., see Ide *et al.*, 1996). Therefore, the researchers involved have collected an enormous amount of high-quality data, providing the means for the validation and possible further improvement in the current methods proposed for performing EEW actions.

We will first summarize the characteristics of the selected data set, as well as delineate the main steps carried out in the analysis of the data by the GFZ-Sentry software. We will then analyze the results, discussing the performance of the software in terms of both possible improvements and the efficiency and added benefits that a DOSEW system (running the GFZ-Sentry software) could provide for areas that have been affected by seismic events of strong to major magnitude.

DATA SET

The data set used here is composed of 3,225 three-component recordings from 24 seismic events; it was obtained by the K-NET and KiK-net surface stations between 1997 and 2011. Together, these networks constitute the National Research Institute for Earth Science and Disaster Prevention (NIED), a nationwide strong-motion network that was established just after the 1995 Kobe earthquake. The resolution of the installed instruments is less than 10^{-4} cm/s^2, and the maximum recordable accelerations during the data collection period were $2g$ for the KiK-net and $4g$ for the K-NET network. The overall frequency response is flat from d.c. to 30 Hz (Fujiwara *et al.*, 2004). The sampling rate of the stations was either 100 or 200 samples/s, depending on the station.

The magnitudes of the selected earthquakes range from 6.0 to 7.3 M_{JMA} (M_w 5.7 and 6.9, with moment magnitudes M_w obtained from the NIED centroid moment tensor solutions catalog, see Data and Resources) and the hypocentral (epicentral) distances range between 5 and 107 km (2 and 103 km, respectively). These values have been chosen in order to include events that are capable of generating shaking that is significant enough to cause damage to built structures (seismic intensity greater than or equal to modified Mercalli intensity [MMI] V), but to still remain within the range of validity of the peak ground displacement (Pd)–peak ground velocity (PGV) relationship adopted in this study (Zollo *et al.*, 2010). In fact, the Zollo *et al.* (2010) relationship was obtained using 3,552 recording of 296 events from Japan, Taiwan, and Italy. Those events had magnitudes between 4 and 8.5 and epicentral distances from a few kilometers to 150 km. However, most of the records were acquired at epicentral distances of less than 60 km and had magnitudes of less than 7, similar to the range considered in the current work. For this reason, large magnitude events that occurred within the considered period of time have not been used. Although Carranza *et al.* (2013) showed that the Zollo *et al.* (2010) relationship can be extended to lower magnitudes and larger hypocentral distances, these are combinations that provide ground-motion values that are not likely to induce any damage and therefore have not been considered in this study.

BASIC PRINCIPLES OF THE TESTED DOSEW SOFTWARE

The time series of ground motion recorded by the stations of the K-NET and KiK-net networks have been analyzed using a damage-forecasting approach based on an empirical relationship procedure proposed by Parolai *et al.* (2015). The procedure can be summarized as follows.

First, a low-pass filter (corner frequency at 1 Hz) is applied recursively during the data acquisition. Then, a standard short-time average over long-time average (STA/LTA) time-domain algorithm is used to identify a possible seismic event. The STA window is fixed to 0.5 s, whereas the LTA window is set to 6 s.

Data (acceleration) are integrated in real time to velocity and displacement. The Pd (e.g., Wu and Kanamori, 2005) found in the first few seconds (where the maximum time used is 3 s) after the P-wave arrival in the vertical component is used to estimate the PGV (median with associated 16% and 84% confidence intervals) on the horizontal components using empirical relationships. Following Parolai *et al.* (2015), these values are in turn used to estimate the traffic light status (green, orange, red) through the use of three matrices that link the expected ground motion to the possible damage (in seismic intensity) it can cause. In the case at hand, a seismic intensity value of VI (related to a PGV of 8.1 cm/s; Wald *et al.*, 1999) was used as the minimum threshold for the red status, corresponding to the very likely occurrence of slight structural damage. Although the analysis is carried out at a maximum of the first 3 s after the detection of the event, a red alarm can be issued before this time is up. The orange and the green status are defined when the observed ground shaking either ranges between 3.4 and 8.1 cm/s, or is less than 3.4 cm/s, respectively. This means that for a green status, no damage is expected (i.e., intensity less than or equal to IV), whereas for an orange status, very light damage may occur (i.e., intensity V).
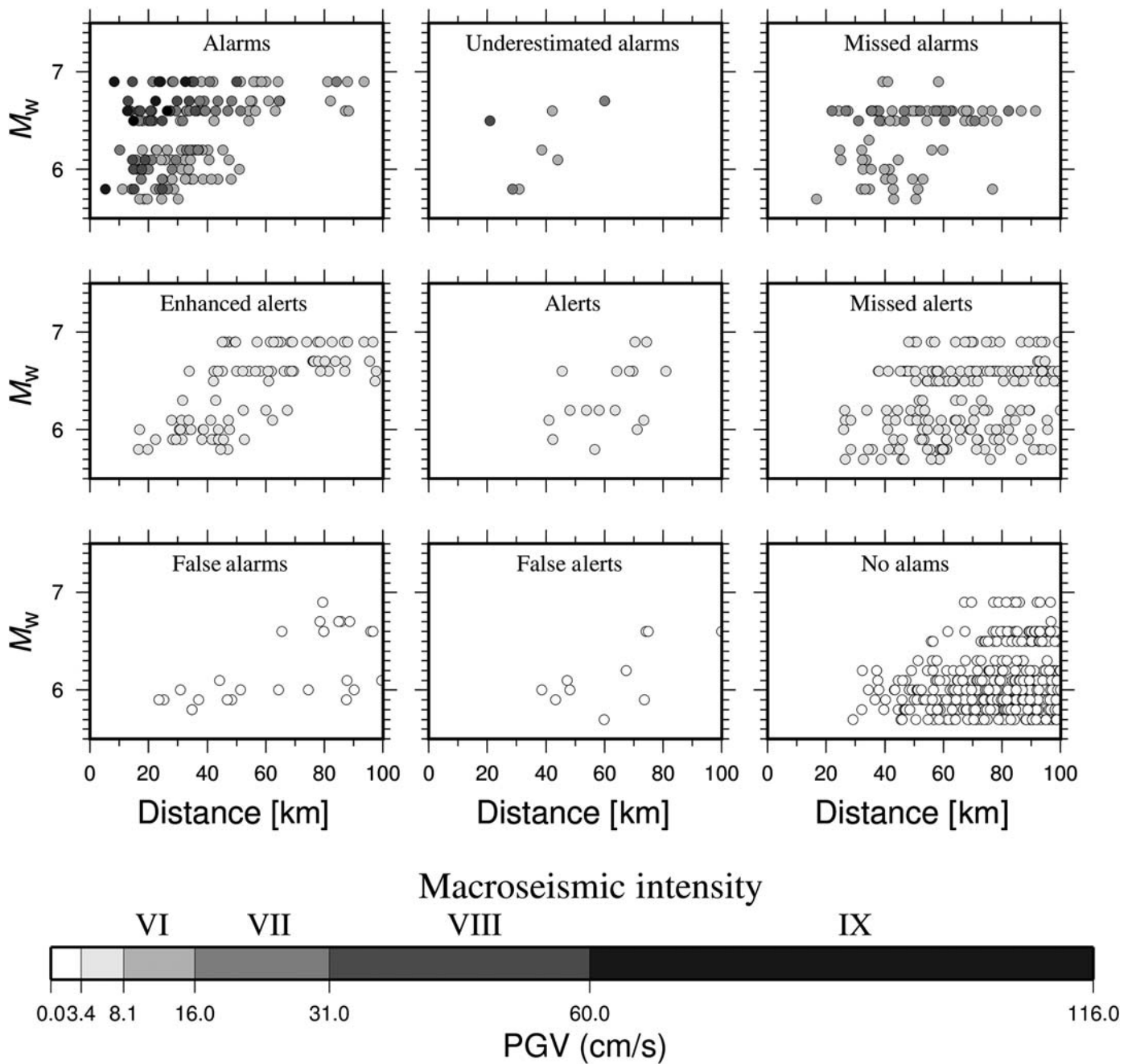
RESULTS

Performance in Alarming

To interpret the obtained results, we present them (Fig. 1) by plotting, on several panels, all possible combinations of declared status by the GFZ-Sentry software (columns from left to right indicate declared red, orange, and green alarms, respectively) versus the alarm levels that should have been assigned to the record using the same criteria (lines from top to bottom indicate red, orange, and green alarms, respectively).

For the sake of clarity, we define
- Alarms (first column, first row in Fig. 1): recordings for which a red status was correctly forecast;
- Underestimated alarms (second column, first row in Fig. 1): recordings for which an orange status was forecast when it should have been classified as red;

▲ **Figure 1.** The results obtained by the software while analyzing the selected recordings shown as a function of hypocentral distance and magnitude M_w. The gray scale indicates the maximum peak ground velocity (PGV), as well as the corresponding seismic intensity observed from the two horizontal components of motion. Each panel represents different combinations of statuses declared by the software (by analyzing up to a maximum of 3 s after triggering) and the observed PGV. See the Results section for further details.

- Missed alarms (third column, first row in Fig. 1): recordings for which a green status was forecast when it should have been classified as red;
- Enhanced alerts (first column, second row in Fig. 1): recordings for which a red status was forecast when it should have been classified as orange;
- Alerts (second column, second row in Fig. 1): recordings for which an orange status was correctly forecast;

- Missed alerts (third column, second row in Fig. 1): recordings for which a green status was forecast when it should have been classified as orange;
- False alarms (first column, third row in Fig. 1): recordings for which a red status was forecast when it should have been classified as green;
- False alerts (third column, second row in Fig. 1): recordings for which an orange status was forecast when it should have been classified as green; and

- No alarms (third column, third row in Fig. 1): recordings for which a green status was correctly forecast.

For each panel, we have plotted the magnitude (M_w)–(hypocentral distance) combination for a given station arising from a given event that gives that alarm/alert status.

Based on the used data set and the adopted criteria, 63% of the red statuses (among a total of 231) were classified correctly as alarms, 3% were assigned to the orange status (underestimated alarms), and 34% were assigned to the green status (missed alarms). Among the latter, however, only 19 recordings (6% of the total) would have corresponded to an observed intensity of VII (moderate damage), whereas the remaining majority would still have been at an observed intensity of VI, which is associated with only slight structural damage. This performance is fair if we consider that recently, Kodera *et al.* (2016) showed that even the Japanese regional early warning system, which relies on multiple recordings, underestimates the Japan Meteorological Agency (JMA) seismic intensity by one degree of intensity in 10% of cases. Using the reference MMI VI as defined in this study, which corresponds to a JMA intensity level of 5 (Kodera *et al.*, 2016), an underestimation of one degree on the JMA scale corresponds to an underestimation of two degrees on the MMI scale (this apparent discrepancy in the number of degrees between scales is a result of the fact that the number and width of the intervals defined in each intensity scale are very different, see fig. 10 in Kodera *et al.*, 2016).

Figure 1 shows that the 308 orange status levels observed are systematically either enhanced (28%) or missed (66%). This would result in either an alarm followed by no consequences but with a level of shaking that would be felt by the population that is not significant enough to affect their trust in the system (intensity V) or in shaking felt by the population that would not lead to serious consequences and therefore their not belittling the importance of the system (intensity V), respectively.

Looking at the bottom panels of Figure 1, it is clear that only in 5% of the 496 cases where a "no alarm" status was issued should there have been a "false alarm" forecast instead, whereas in 2% of the these cases, a "false alert" should have been declared.

Another way of analyzing the results is to consider the performance of the software by looking at the declared statuses. For example, among all of the 259 declared red statuses (the left column of panels in Fig. 1), in 10% of the cases, the shaking would not have been able to generate any damage; whereas in 34% of the cases (enhanced alerts), some slight damage could have been expected. From this perspective, the issuing of a red status is followed in 90% of cases by shaking leading to a seismic intensity equal to or greater than V (very light potential damage). All the recordings that should have led to an intensity greater than VII have been correctly classified by a red status.

Similarly, when focusing on all of the 741 declared green statuses (right column of panels in Fig. 1), it is remarkable that in only 10% of the cases did a "missed alarm" occur, whereas in only 2.5% of the cases, the missed alarms missed the occurrence of a seismic intensity equal to VII (moderate damage). In 27%

of the cases (missed alerts), a declared green status could have been followed by an intensity level equal to V (very light potential damage).

Looking at the distribution of the data in the "alarm" (top left) and "no alarm" (bottom right) panels, one can identify a clear separation between the two statuses as a function of magnitude–distance combination (Fig. 1), at least in the majority of the analyzed cases. Generally, higher magnitude and closer events led to alarms, whereas lower magnitude and more distant events led to the "no alarm" status.

Finally, although the declaration of an orange status seems to be less valuable, it is worth noting that only in 20% of the cases would this have led to an underprediction of the potential damage (intensities between VI and VII). Additionally, the declaration of the orange status would have been followed by intensities equal to VII in only 8% of the cases. Although the orange status might be of importance during the occurrence of the shaking to monitor the evolution of the event, it might be less relevant in terms of actions following the real-time decision-making procedure.

Figure 2 shows the predicted and observed level of shaking for the possible different statuses and clarifies that the poor performance of the software in defining the orange status, for the selected combination of the Pd to PGV relationship and adopted thresholds, is due to the large standard deviation of the relationship with respect to the chosen threshold interval (Parolai *et al.*, 2015). In fact, a small variation in the predicted median and the corresponding 84% percentile leads to a jump from the green to the red status. The performance could therefore be improved by either better calibration of the threshold levels or by the introduction of locally derived Pd to PGV relationships (which would likely be less affected by scattering in the data). Alternatively, a probabilistic approach, as introduced by Parolai *et al.* (2015), could be considered to define the status. The range of predicted values of shaking in the left column panels (alarms, enhanced alerts, and false alarms) for the different events does not show significant variability. This, of course, is due to the fact that as soon as the predicted values are large enough to see a red status issued, the procedure is stopped.

Furthermore, the top left panel suggests that the ground motion predicted for reaching the "alarm" status is generally followed by much more significant shaking. Figure 3 shows examples of the displacement and velocity recordings of two strong events, the 2000 M_w 6.6 Tottori (e.g., Pulido and Kubo, 2004; Fig. 3a,b) and the 2003 M_w 6.1 Miyagi-Oki (e.g., Miuara *et al.*, 2004; Fig. 3c,d) events, respectively. These were recorded at different hypocentral distances. In all the considered cases, a red alarm status was correctly declared well before the maximum allowed signal window length of 3 s was reached. Consistent with the findings of Parolai *et al.* (2015), the level of ground velocity that could lead to slight damage (8.1 cm/s, black triangles) is overstepped well after the arrival of the S waves (white triangle), increasing the available lead time. The S-wave arrival times for all the recordings were estimated either by automatic picking or, in case only a P onset could be picked
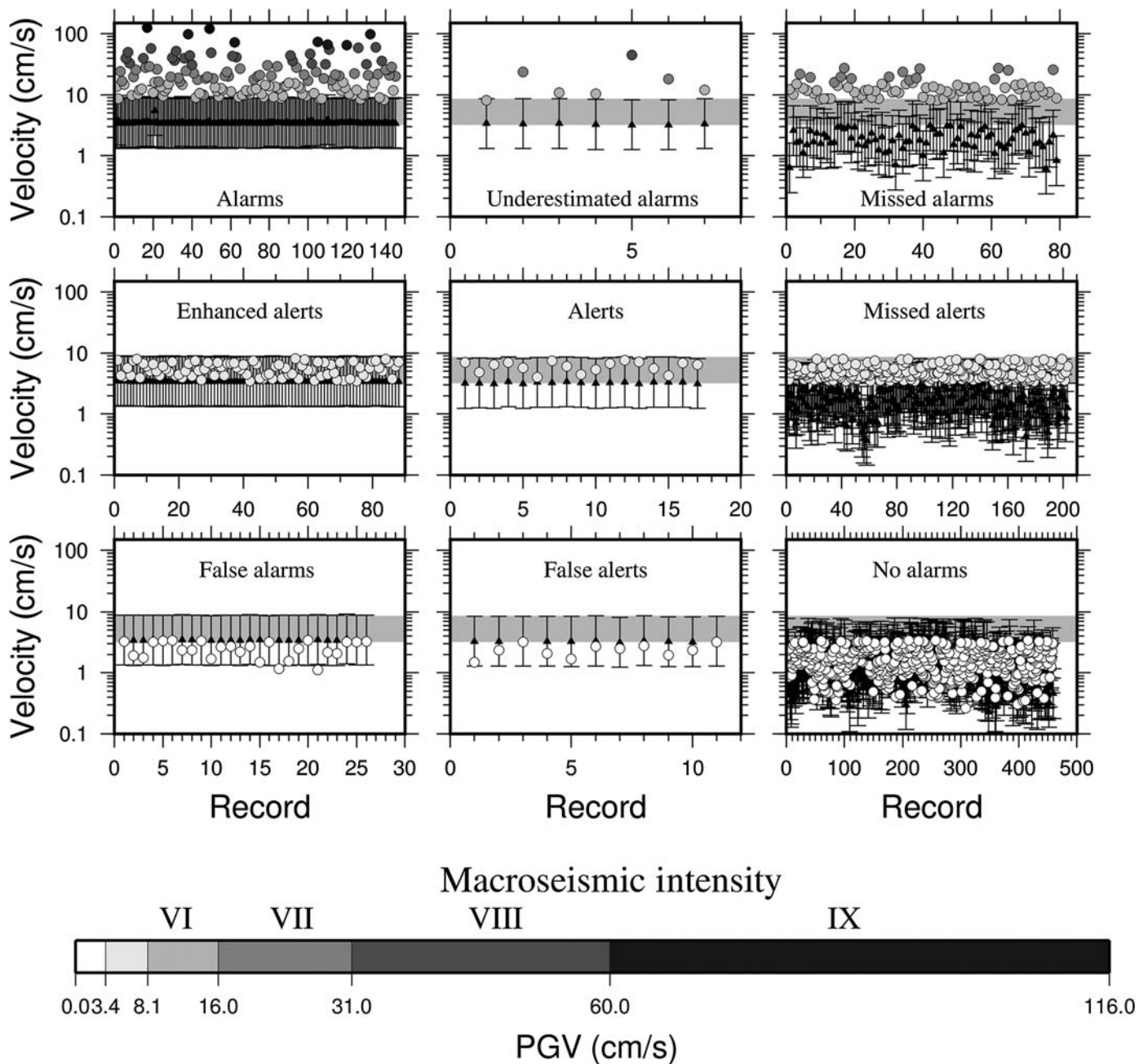
▲ **Figure 2.** The results obtained by the software as a function of the number of recordings (progressive for each category) and observed PGV. The gray scale indicates the maximum PGV (and the corresponding seismic intensity) observed from the two horizontal components of motion. Each panel shows the results for different combinations of statuses declared by the software and the observed PGV. The light gray area is representative of the values between the chosen 3.4 and 8.1 cm/s velocity thresholds on the graph. The median and 16% and 84% confidence intervals that were estimated by the software for each analyzed recording are indicated by the black triangles and the vertical black lines, respectively. See the Results section for further details.

automatically, by calculating the S-wave arrival time using the JMA 2001 velocity model (Oth, Parolai, *et al.*, 2011). In the case of the M_w 6.6 2000 Tottori earthquake recorded from a distance of 17 km, the time difference between the declaration of the alarm and the occurrence of the significant shaking would still allow for the application of automatic shutdown systems at critical facilities.

Figure 4 shows examples of the displacement and velocity recordings of two strong events, the 2000 M_w 6.6 Tottori (Fig. 4a,b) event once again, and the 1997 M_w 6.0 Kagoshima-2 (e.g., Horikawa, 2001; Fig. 4c) event. These events were recorded at different hypocentral distances, and in both cases, a red alarm status was erroneously not declared. In each of these cases, a rather small low-frequency content is
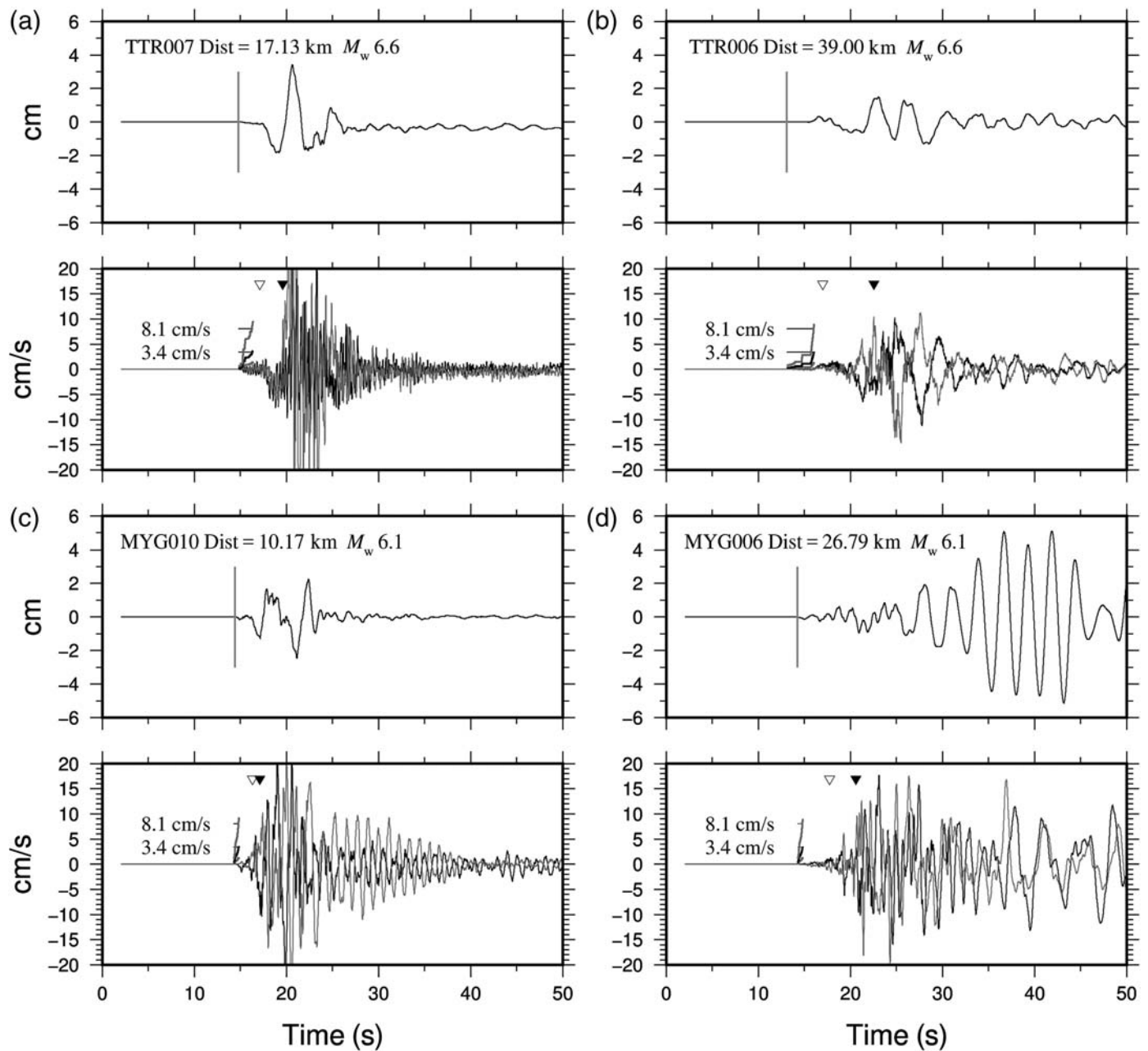
▲ **Figure 3.** The results for four different recordings for which the Alarm status was declared. Lower panels in (a)–(d): The predicted PGV values (84% and 16% confidence intervals in gray and the mean in black) estimated from the vertical component and the east–west (black) and north–south (gray) velocity recordings. The horizontal gray lines indicate the threshold values used in the traffic light procedure, set to 3.4 and 8.1 cm/s, respectively. Top panels in (a)–(d): The displacement (black line) recordings and the trigger time (vertical gray line). The white triangles indicate the theoretical arrival time of the S waves. The black triangles indicate when the 8.1 cm/s threshold is overstepped.

observed in the first 3 s after the trigger. The displacement at Station SMN002 (Fig. 4b) is only slightly less than what is observed at Station TTR007 (Fig. 3a). These differences lead to the declaration of the red alarm status for TTR007. However, the ground velocity at SMN002 is much larger and richer in higher frequencies (yet still lower than 1 Hz) and shows a long-shaking duration at nearly 0.5 Hz. This is consistent with the low V_{S30} (average S-wave velocity in the uppermost 30 m)

measured at the SMN002 station (138 m/s) and the larger amplification at frequencies lower than 1 Hz (Oth, Bindi, et al., 2011), with respect to that estimated at TTR007 ($V_{S30} = 469$ m/s). The missed alarm may therefore be due to the occurrence of the amplification of the S waves at site SMN002. This problem could be easily solved by recalibrating the adopted thresholds to account for the occurrence of site effects at this or other sites. The recording at Station
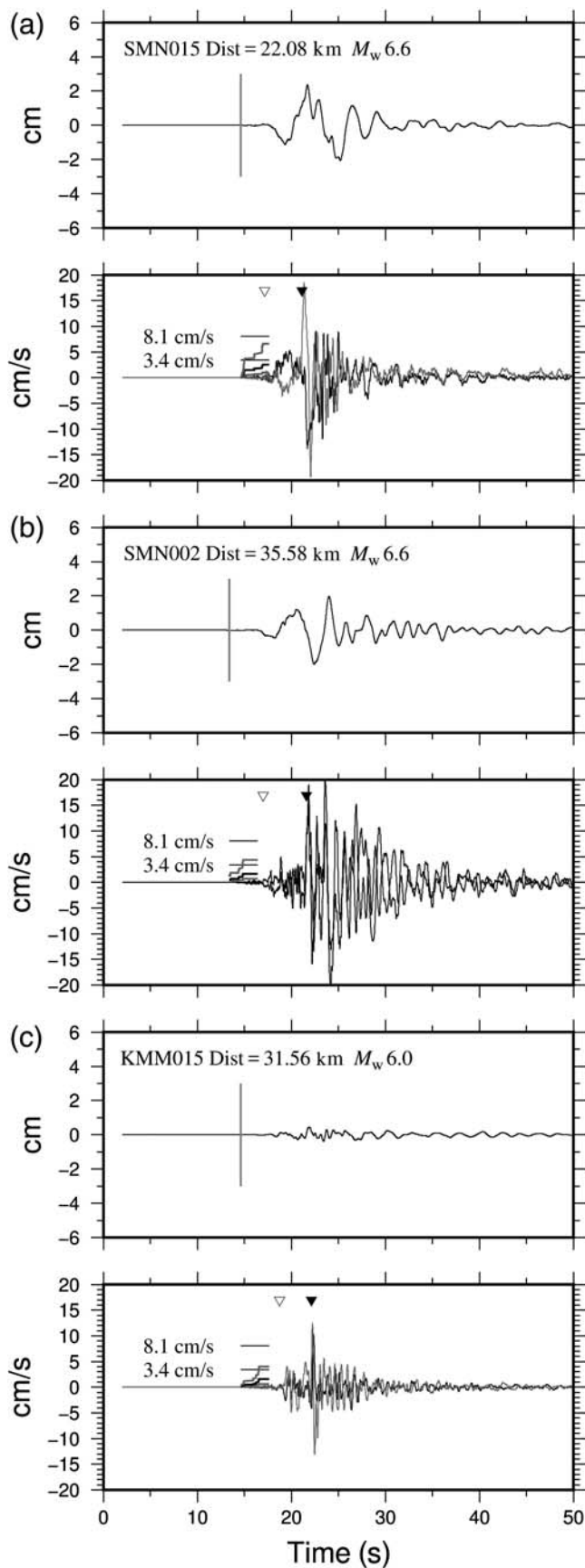
▲ **Figure 4.** Same as Figure 3, but for three different recordings for which a missed alarm occurred.

KMM015 shows a surprisingly small low-frequency content, especially when compared with the recording at station MYG006 (Fig. 3d) that was collected for an event of similar magnitude and distance. This kind of peculiarity is responsible for the underestimation of the expected shaking in this case. Figure 5 shows the displacement and velocity data of strong events recorded at different hypocentral distances/stations (a, NIGH05; b, TYM004; c, AKT022; d, KMM016) for which a red status was erroneously declared. The false alarm status at the Stations NIGH05 (2004 M_w 6.0 Mid-Niigata-2 event) and KMM016 (1997 M_w 6.0 Kagoshima-2 earthquakes), which are both good representations of such cases (although these cases are rare), is due to a problem in the baseline correction in the simulated real-time procedure. In fact, the baseline correction is carried out during the short running signal windows before the low-pass filtering (Parolai *et al.*, 2015), but unlike the real-time procedure, there is no recursive control that would correctly remove the residual displacement. We assume that this lack of recursive control is responsible for the large overestimation of the expected ground velocity in these few cases. The false alarm issued at Station TYM004 (2007 M_w 6.7 Noto earthquake) is due to both anomalous low-frequency content (which is nearly monofrequent at ∼0.3 Hz), and high-amplitude ground displacement in the *P*-wave coda (which actually appears to be very poor in the high-frequency content). Similarly, at Station AKT022 (1998 M_w 5.9 earthquake), the shown waveform is particularly rich in low-frequency content with respect to the higher frequencies for both *P* and *S* waves. In all of these cases, even if it was unlikely that structural damage would occur, the issuing of a false alarm would not induce any "cry wolf" feelings within the population. In fact, the observed values are still within the lower boundary of one standard deviation of the forecast amount of earthquake shaking and are sufficient to be felt by the general population.

Figure 6 shows the displacement and velocity recordings of the 2008 M_w 6.9 Iwate event (e.g., Cultrera *et al.*, 2013), recorded from a distance of nearly 80 km. A green status was correctly declared for this event. These recordings show a combination of magnitude and distance that is approaching the boundary between the red and the green statuses, which we have seen is very close (see Fig. 1). This figure shows that the highest level of shaking is related to the lower-frequency (around 0.17 Hz) surface-wave arrival, which stands in agreement with the predicted median value regardless. This level of shaking would possibly be felt by the population, but it would be very unlikely to generate even slight damage. Therefore, if the information from the early warning systems is correctly communicated, the trust in the system could even be strengthened.

Actual Lead Time
Generally, the usefulness of an early warning system is also evaluated by considering the lead time that can be achieved, which could constrain the size of the so-called blind zone (i.e., the area that cannot receive warnings in time). The lead
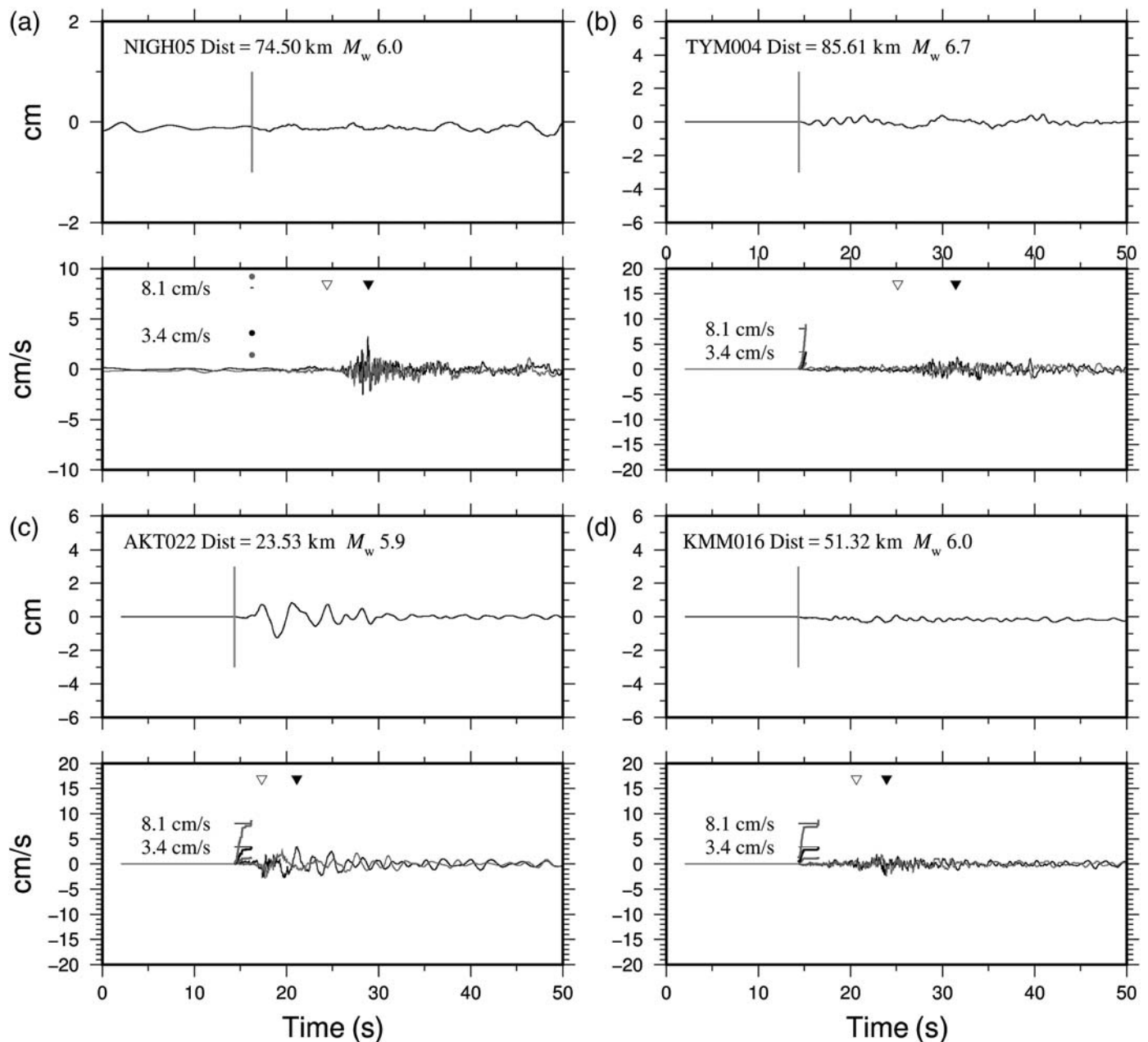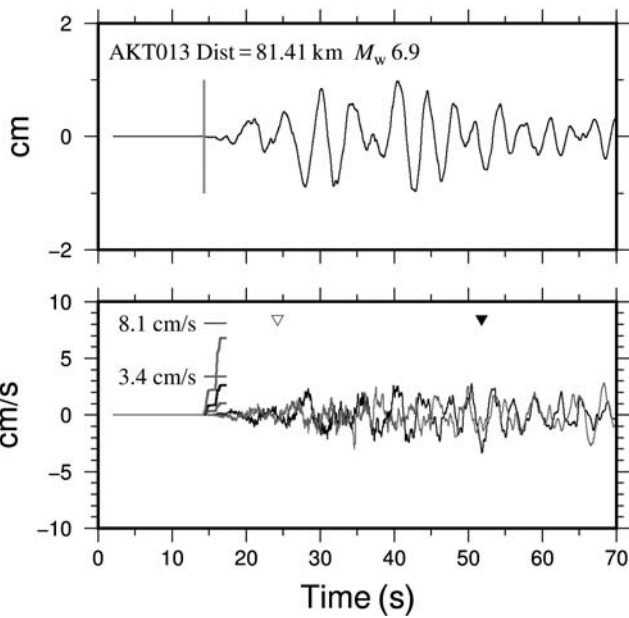
▲ **Figure 5.** Same as Figure 3, but for which a false alarm occurred.

time is estimated as the time between the issuing of the alarm (T_{alarm}) and the arrival of the damaging waves, which, for the sake of simplicity, is very often chosen in such a way that it coincides with the S-wave arrival (T_{S_waves}).

On the basis of a few available events, Parolai *et al.* (2015) suggested that the lead time might be significantly larger than expected if, considering the choice made when defining the alarm thresholds, the arrival time of damage coincides with the first time that the ground velocity oversteps the value corresponding to the likely occurrence of slight structural damage (here defined as 8.1 cm/s, $T_{threshold\_8.1\_cm/s}$). Specifically, this might have important consequences with regard to possibilities for implementing automatic safety procedures (e.g., shutdown)

in the event of larger earthquakes at short hypocentral distances (< 20 km). The top left panels of Figure 3 appear to confirm this suggestion even for major events, showing that the lead time might be larger by nearly 2.5 s with respect to the expectation when considering the arrival of the S waves.

Figure 7 compares the differential times between T_{S_waves} and T_{alarm} with those between $T_{threshold\_8.1\_cm/s}$ and T_{alarm} for the recordings that have been classified as Alarms (top, left panels in Figs. 1 and 2). The gray scale in the figure indicates the hypocentral distances of the used recordings. There is a tendency for $T_{threshold\_8.1\_cm/s} - T_{alarm}$ to increase with distance, which is related to the fact that for larger hypocentral distances, the largest ground velocity can be a result of later arrivals, such

▲ Figure 6. Same as Figure 3, but for which a "no alarm" was correctly estimated.

as surface waves. Furthermore, we notice that 75% of the $T_{\text{threshold\_8.1\_cm/s}} - T_{S\_\text{waves}}$ times (measured as the orthogonal distance of each point from the diagonal black line) are greater than 1 s and that 65% of these times range between 1 and 5 s.
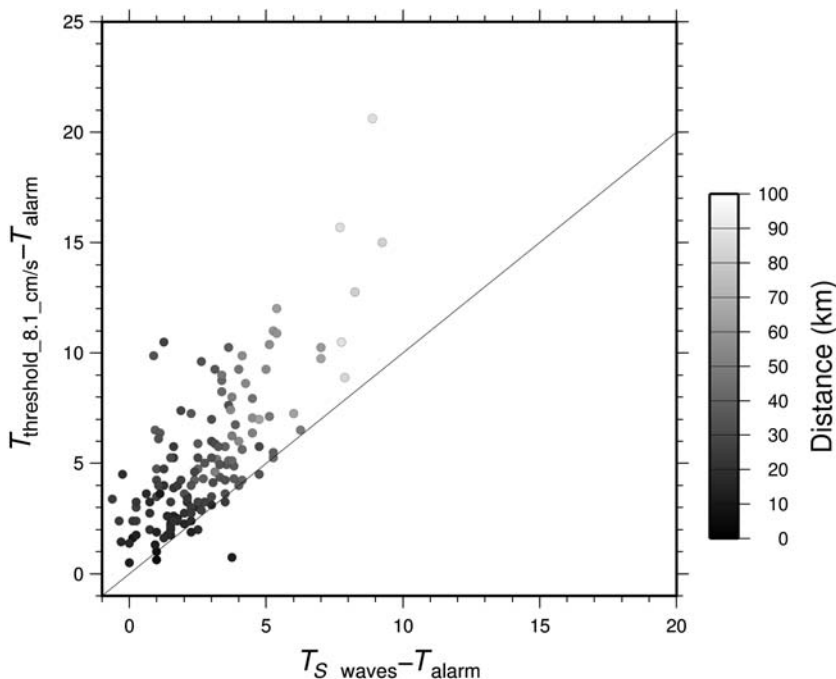
▲ Figure 7. For the recordings that have been classified as Alarms, the differential time between the theoretical arrival of the S waves (T_{S_waves}) and the issuing of the alarm (T_{alarm}) versus the differential time between the ground velocity overstepping the fixed threshold of 8.1 cm/s ($T_{\text{threshold\_8.1\_cm/s}}$) and T_{alarm} (top, left panels in Figs. 1 and 2). The gray scale in the figure indicates the hypocentral distances of the plotted recordings.

These results support the idea that decentralized on-site earthquake early warning can have greater potential than previously expected in terms of promptly providing information that is useful for quick actions. It could be used to dramatically reduce the blind zone (especially when automatic actions for industrial and critical facilities are necessary) in areas where only sparse networks are available for regional early warning systems.

DISCUSSIONS AND CONCLUSIONS

In this article, we reported on the application of the GFZ-Sentry software that is meant to function in decentralized on-site earthquake early warning. It was tested on a large data set of recordings collected by the K-NET and KiK-net surface stations in Japan. The performance of the software, evaluated without making *ad hoc* calibrations for the area or for the selected thresholds, has proven to be more than fair. Only in 10% of the cases was an issued red status not followed by damaging shaking, and it was less than 10% of cases that involved a green status being followed by potentially damaging shaking. It could be that in some of these cases the maximum allowed window length of 3 s is not sufficient to capture the maximum Pd related to the event, therefore leading to an underestimation of its potential shaking. False alarms were issued in only 5% of the cases, and this number is likely to be lower when the procedure is run in a real-time mode because a recursive control would remove the residual displacement that is causing the current shortcoming of the analysis. The results, however, showed poorer performance in forecasting intermediate orange statuses. This performance could potentially be improved by either introducing site-specific Pd-to-PGV relations or optimizing the choices in terms of the threshold values. The performance could also be improved by adopting probabilistically based definitions of the status (as proposed by Parolai *et al.* (2015)) but only after having carried out an extensive probabilistic cost–benefit analysis at each site. These analyses would involve the evaluation of the conditional probabilities associated with certain statuses, as well as the occurrence of a certain level of ground motion.

Additionally, attempts can be made in the future to directly estimate the JMA intensity by considering locally derived PGV–intensity relations (e.g., Karim and Yamazaki, 2002). However, considering the short time in which actions should be included in a DOSEW system, it would probably also be worthwhile to explore the possibility of simplifying the system (depending on possible end users and customers) into a simple binary system where only green and red statuses are issued.

The results shown in this article confirmed that a DOSEW system is able to launch an

alarm and trigger automatic actions before the inception of damaging shaking. We showed that the damaging shaking generally arrives after the *S*-wave arrival, providing further precious seconds for taking actions, even for major events and at distances shorter than 20 km. It is clear that a combination of DOSEW systems (which can utilize low-cost instruments, as shown by Clinton *et al.*, 2016) with regional systems could have a great deal of potential, both for reducing the blind zone and for combining actions that are useful for the general population and critical facilities. However, considering the short lead time that EEW (particularly on-site EEW) can deliver, the implementation of these systems would have to be accompanied by activities that facilitate a better comprehension of their functioning (including success and possible failures). These activities should also serve the purpose of increasing the awareness and preparedness of the population and end users as to the value and limitations of the systems.

The GFZ-Sentry software is now running in real-time operational mode on the real-time strong-motion networks that the Helmholtz Center Potsdam GFZ German Research Center for Geosciences (GFZ) is operating in cooperation with local partners in Central Asia, Greece, and Turkey. The performance of the software will therefore be better evaluated on the day-by-day operations, and the possibility of improving it through regionally oriented and site-specific corrections will be investigated.

DATA AND RESOURCES

The seismograms used in this study were collected from the National Research Institute for Earth Science and Disaster Prevention (NIED) in Japan. Data can be obtained from the K-NET and KiK-net websites at http://www.kyoshin.bosai.go.jp/ (last accessed August 2017). Information about the ACROSS network can be derived from the Helmholtz Centre Potsdam GFZ German Research Centre for Geosciences (GFZ) (http://lhotse.gfz-potsdam.de/nagvis/frontend/nagvis-js/index.php?mod=Map&act=view&show=across, last accessed August 2017). The NIED centroid moment tensor (CMT) solutions catalog is accessible via http://www.fnet.bosai.go.jp/top.php (last accessed August 2017). ⊠

ACKNOWLEDGMENTS

REFERENCES

Aoi, S., T. Kunugi, H. Nakamura, and H. Fujiwara (2011). Deployment of new strong motion seimographs of K-NET and KiK-net, in *Earthquake Data in Engineering Seismology*, T. Van Eck, P. Gülkan, and S. Akkar (Editors), Springer, Heidelberg, Germany.

Bindi, D., T. Boxberger, S. Orunbaev, M. Pilz, J. Stankiewicz, M. Pittore, I. Iervolino, E. Ellguth, and S. Parolai (2015). On-site early-warning system for Bishkek (Kyrgyzstan), *Ann. Geophys.* **58,** no. 1, doi: 10.4401/ag-6664.

Bindi, D., I. Iervolino, and S. Parolai (2016). On-site structure-specific real-time risk assessment: Perspectives from the REAKT project, *Bull. Earthq. Eng.* **14,** no. 9, 2471–2493, doi: 10.1007/s10518-016-9889-4.

Carranza, M., E. Buforn, S. Colombelli, and A. Zollo (2013). Earthquake early warning for southern Iberia: A *P* wave threshold-based approach, *Geophys. Res. Lett.* **40,** 4588–4593.

Clinton, J., A. Zollo, A. Marmureanu, C. Zulfikar, and S. Parolai (2016). State-of-the art and future of earthquake early warning in the European region, *Bull. Earthq. Eng.* **14,** no. 9, 2441–2458.

Cultrera, G., G. Ameri, A. Sarao, A. Cirella, and A. Emolo (2013). Ground-motion simulations within ShakeMap methodology: Application to the 2008 Iwate-Miyagi Nairiku (Japan) and 1980 Irpinia (Italy) earthquakes, *Geophys. J. Int.* **193,** 220–237, doi: 10.1093/gji/ggs074.

Fujiwara, H., S. Aoi, T. Kunugi, and S. Adachi (2004). Strong motion observation networks of NIED: K-NET and KiK-net, *Cosmos Report*, National Research Institute for Earth Science and Disaster Prevention, Japan.

Horikawa, H. (2001). Earthquake doublet in Kagoshima, Japan: Rupture of asperities in a stress shadow, *Bull. Seismol. Soc. Am.* **91,** 112–127, doi: 10.1785/0119990131.

Ide, S., M. Takeo, and Y. Yoshida (1996). Source process of the 1995 Kobe earthquake: Determination of spatio-temporal slip distribution by Bayesian modeling, *Bull. Seismol. Soc. Am.* **86,** 547–566.

Karim, K. R., and F. Yamazaki (2002). Correlation of JMA instrumental seismic intensity with strong motion parameters, *Earthq. Eng. Struct. Dynam.* **31,** 1191–1212.

Kodera, Y., Y. Yamada, S. Adachi, M. Morimoto, Y. Nishimae, and M. Hoshiba (2016). The eight years of earthquake early warning operation in the Japan Meteorological Agency, in *Earthquake and Induced Multi-Risk Early Warning and Rapid Response*, in Cahier du Centre Europeen de Geodynamique et de seismologie, A. Oth and S. Parolai (Editors), Vol. 31, 17–30.

Miuara, S., Y. Suwa, T. Sato, K. Tachibana, and A. Hasegawa (2004). Slip distribution of the 2003 northern Miyagi earthquake (M 6.4) deduced from geodetic inversion, *Earth Planets Space* **56,** 95–101.

Okada, Y., K. Kasahara, S. Hori, K. Obara, S. Sekiguchi, H. Fujiwara, and A. Yamamoto (2004). Recent progress of seismic observation networks in Japan-Hi-net, F-net, K-NET and KiK-net, *Earth Planets Space* **56,** 15–28.

Oth, A., and S. Parolai (2016). *Earthquake and Induced Multi-Risk Early Warning and Rapid Response*, in Cahier du Centre Europeen de Geodynamique et de seismologie, A. Oth and S. Parolai (Editors), Vol. 31.

Oth, A., D. Bindi, S. Parolai, and D. Di Giacomo (2011). Spectral analysis of K-NET and KiK-net data in Japan, part II: On attenuation characteristics, source spectra, and site response of borehole and surface stations, *Bull. Seismol. Soc. Am.* **101,** 667–687, doi: 10.1785/0120100135.

Oth, A., S. Parolai, and D. Bindi (2011). Spectral analysis of K-NET and KiK-net data in Japan, part I: Database compilation and peculiarities, *Bull. Seismol. Soc. Am.* **101,** 652–666, doi: 10.1785/0120100134.

Parolai, S., D. Bindi, T. Boxberger, C. Milkereit, K. Fleming, and M. Pittore (2015). On-site early warning and rapid damage forecasting

using single stations: Outcomes from the REAKT project, *Seismol. Res. Lett.* **86,** no. 5, 1393–1404, doi: 10.1785/0220140205.

Pulido, N., and T. Kubo (2004). Near-fault strong motion complexity of the 2000 Tottori earthquake (Japan) from a broadband source asperity model, *Tectonophysics* **390,** 177–192.

Strauss, J. A., and R. M. Allen (2016). Benefits and costs of earthquake early warning, *Seismol. Res. Lett.* **87,** no. 3, 765–772, doi: 10.1785/0220150149.

Wald, D. J., V. Quitoriano, T. H. Heaton, and H. Kanamori (1999). Relationship between peak ground acceleration, peak ground velocity, and modified Mercalli intensity in California, *Earthq. Spectra* **15,** 557–564.

Wenzel, F., and J. Zschau (2014). *Early Warning for Geological Disasters: Scientific Methods and Current Practice*, Springer-Verlag, Berlin, Germany.

Wessel, P., and W. H. F. Smith (1991). Free software helps map and display data, *Eos Trans. AGU* **72,** 445–446.

Woo, G., M. Gobbato, and N. Shome (2016). The cost effectiveness of a West Coast earthquake early warning system, in *Earthquake and Induced Multi-Risk Early Warning and Rapid Response*, in Cahier du Centre Europeen de Geodynamique et de seismologie, A. Oth and S. Parolai (Editors), Vol. 31, 101–112.

Wu, Y.-M., and H. Kanamori (2005). Experiment on an onsite early warning method for the Taiwan early warning system, *Bull. Seismol. Soc. Am.* **95,** 347–353.

Zollo, A., O. Amoroso, M. Lancieri, Y.-M. Wu, and H. Kanamori (2010). A threshold based earthquake early warning using dense accelero-metric networks, *Geophys. J. Int.* **183,** 963–974, doi: 10.1111/j.1365-246X.2010.04765.x.

Stefano Parolai
Tobias Boxberger
Center for Early Warning Systems Section
Helmholtz Centre Potsdam
GFZ German Research Centre for Geosciences
Telegrafenberg
14473 Potsdam
Germany
parolai@gfz-potsdam.de
tobias.boxberger@gfz-potsdam.de

Adrien Oth
European Center for Geodynamics and Seismology
19, rue Josy Welter
L-7256 Walferdange
Grand Duchy of Luxemburg
adrien.oth@ecgs.lu